Effect of an oblique and constant magnetic field in the sheath thickness, the floating potential and the saturation current collected by a planar wall

2014 Plasma Sources Sci. Technol. 23 035012

(http://iopscience.iop.org/0963-0252/23/3/035012)

IOP Publishing Plasma Sources Science and Technology

Plasma Sources Sci. Technol. **23** (2014) 035012 (8pp) doi:10.1088/0963-0252/23/3/035012

Effect of an oblique and constant magnetic field in the sheath thickness, the floating potential and the saturation current collected by a planar wall

R Morales Crespo[1] **and R N Franklin**[2]

[1] Dpto. de Física, Universidad de Córdoba, Campus Universitario de Rabanales, Ed. C2. 14071 Córdoba, Spain
[2] Department of Astronomy and Physics, The Open University, Milton Keynes, UK

E-mail: rutphysics@gmail.com and raoulnf1935@gmail.com

Received 14 March 2014
Accepted for publication 9 April 2014
Published 19 May 2014

Abstract

This work studies the sheath close to a negatively polarized wall in an oblique and constant magnetic field. We also consider ionization and collisions and study the effect of the different pre-sheath mechanisms on such properties as the current to voltage characteristics, the saturation current collected by the wall, the floating potential and the sheath thickness. This last property being the most sensitive to the change in the dominant pre-sheath mechanism which allows the sheath to form.

Keywords: plasma–sheath, floating potential, Langmuir probe, magnetic field, sheath thickness

1. Introduction

In recent years, several papers have been published describing the plasma–sheath transition when a negative polarized wall is immersed in a plasma under the action of a constant magnetic field. Among these works is the Chodura's model, which describes the pre-sheath of a collisionless plasma in an oblique magnetic field [1]. In his model, Chodura shows that there exists a magnetic pre-sheath, called the Chodura layer, where the ions enter with a velocity parallel to the magnetic field equal to the sound speed. After this layer, there is the sheath, a collisionless charged region that begins when the component of the positive ion velocity perpendicular to the wall reaches the sound speed. In the Chodura layer, the electric field grows causing the velocity of the positive ions to deviate from the magnetic-field lines. Several authors extend this model including collisions as a pre-sheath mechanism [2–6], ionization [7] or both ionization and collisions [8]. In the last years, the use of the Boltzmann relation for the electrons when there is a magnetic field parallel to the wall has been re-examined by several authors [9, 10]. This relation is still valid when the electron current flowing to the sheath is very small [9] ($v^2/c_s^2 \ll m_e/M$, where v is the electron flow velocity, c_s is the Bohm velocity and m_e, M are the mass of the electrons and ions, respectively) or when the electron Hall parameter ($eB_\parallel/m_e\nu_{ce}$) is very small [10].

Due to various applications, it is important to study the relationship between the plasma–sheath transition and the different plasma parameters. This paper studies some physical properties of a negatively polarized wall introduced into an electropositive plasma with a constant magnetic field. The three pre-sheath mechanisms involved in the sheath formation are ionization, collisions and magnetization. These mechanisms determine such properties as the current density to voltage characteristics, the saturation current density of the positive ions, the floating potential and the sheath edge which are very important in different experimental applications. Therefore, the model we present here considers what effects on these properties the three pre-sheath mechanisms above mentioned have. To this end, in section 2, we develop the equations of the model using a fluid or hydrodynamic picture. These equations are solved only considering the quasi-neutrality condition, without imposing any extra criterion such as the Bohm criterion. In section 3, a formalism is used that allows us to analyse how these properties change for all possible values of the ionization and collisionality

degree and the magnetic strength. In section 4, after the numerical resolution of the model, the current density to voltage characteristics, the saturation current density for the positive ions, the floating potential and the sheath thickness are analysed according to the corresponding prevailing pre-sheath mechanism.

2. The model

To describe the sheath close to a negatively polarized wall with a constant magnetic field that lies in a plane perpendicular to the wall, we consider the positive ions as a fluid described by the continuity equation

$$\vec{\nabla}(n_+\vec{v}_+) = \nu_i n_e \tag{1}$$

and the momentum transfer equation:

$$M_+ n_+(\vec{v}_+ \cdot \vec{\nabla})\vec{v}_+ + \nu_c M_+ n_+ \vec{v}_+ + \nu_i M_+ n_e \vec{v}_+ = e n_+(\vec{E} + \vec{v} \wedge \vec{B}), \tag{2}$$

where n_+ and $\vec{v}_+$ are the positive ion density and velocity, ν_i and ν_c are the ionization and collision rates, $\vec{E}$ is the electric field and $\vec{B}$ the magnetic field that lies in a plane perpendicular to the wall. The Y–Z directions will be considered parallel to the wall and the X direction perpendicular to it. According to this description the electric and magnetic fields are written as $\vec{E} = E\vec{e}_x$ and $\vec{B} = B(\cos\theta\vec{e}_x + \sin\theta\vec{e}_y)$.

As have been shown by Zimmermann *et al* [10] studying a coaxial discharge with axial magnetic field considering a two fluid model, the validity of the Boltzmann's relation for the electrons has to be re-examined according to the different parameters of the plasma. They have found that if the electron Hall parameter defined by $eB_\parallel/m_e\nu_{ce}$ is small enough, this relation can still be valid, where ν_{ce} is the non-ionizing collision rate for the electrons and $B_\parallel$ is the axial magnetic field parallel to the wall. For values of the electron Hall parameter around 10, only if the ionization rate is small, the Boltzmann relation can be used. Finally, when $eB_\parallel/m_e\nu_{ce} \gg 1$ the error created by the use of the Boltzmann relation can exceed 100%. In the following, we will consider the more restrictive case for which the non-ionizing collision mean free path for the electrons is very small compared with the electron gyroradius ($c_s/\nu_{ce} \ll c_s m_e/eB$). Considering that in our model, the parallel component of the magnetic field is $B_\parallel = B\sin\theta$, the electron Hall parameter as stated in [10] is small enough in order to approximate the electron density by a Boltzmann relation:

$$n_e = n_{e0} e^{e\phi/K_B T_e}, \tag{3}$$

T_e being the electronic temperature and n_{e0} the electronic density at the plasma. Finally, the Poisson equation, together with equations (1)–(3), determines the electric potential profile from the plasma to the wall:

$$\vec{\nabla}^2\phi = -\frac{e}{\varepsilon_0}(n_+ - n_{e0}e^{e\phi/K_B T_e}) \tag{4}$$

where ϕ is the electric potential referred to the plasma potential. In all these equations, and due to the symmetry of the problem, we have considered that all our variables depend on the perpendicular coordinate to the wall surface x. The plasma will be considered to be at the left of the wall. To consider the most general situation, the ion–neutral collision frequency will be taken as a function of the speed of the positive ions in the form $\nu_c(v_+) = n_n c_s \sigma_s (v_+/c_s)^{p+1}$, where n_n is the density of the neutrals and σ_s is the collisional cross-section when the positive ions move at $c_s = \sqrt{K_B T_e/M_+}$ (the Bohm velocity). If $p = -1$, the ion–neutral collision frequency is constant, while if $p = 0$ the mean free path for this process is constant.

3. Normalized model equations

The plasma–sheath transition can be divided into two regions described by two length scales that characterize the physical processes happening in these regions, the pre-sheath and the sheath region. In the pre-sheath region, there are three mechanisms which compete to form the sheath. These mechanisms are also characterized by their own lengths: (i) the mean free path for collisions λ_c, (ii) the mean free path for ionization λ_i and (iii) the magnetic length λ_b for magnetization. All these lengths are given by

$$\lambda_c = \frac{c_s}{\nu_c(c_s)} = \frac{1}{n_n\sigma_s}, \qquad \lambda_i = \frac{c_s}{\nu_i}, \qquad \lambda_b = \frac{c_s M_+}{eB}. \tag{5}$$

From these lengths, the corresponding non-neutrality parameters can also be defined :

$$q_c = \frac{\lambda_D}{\lambda_c}, \qquad q_i = \frac{\lambda_D}{\lambda_i}, \qquad q_b = \frac{\lambda_D}{\lambda_b}. \tag{6}$$

In order to make all the physical constants of the model equal to unity, we normalize the electric potential using the thermal electron energy in the plasma ($-e\phi/K_B T_e$), the spatial coordinate perpendicular to the wall x with the characteristic length of the region to be described L (λ_D for the sheath region, and λ for the pre-sheath region, where λ can be one of λ_c, λ_i, or λ_b depending on the prevailing pre-sheath mechanism). We also use the Bohm speed $c_s = \sqrt{K_B T_e/M_+}$ and electronic density in the plasma n_{e0} to define the dimensionless density and velocity of the positive ions:

$$N = \frac{n_+}{n_{e0}}, \qquad \vec{c} = \frac{\vec{v}_+}{c_s}, \tag{7}$$

where $\vec{c} = (u, v, w)$ and u, v, and w are the normalized components of the positive ion velocity.

3.1. Sheath representation

In the sheath $L = \lambda_D$, and the sheath representation which determines the electric potential in the sheath scale is defined by

$$X = \frac{x}{\lambda_D}, \qquad y(X) = -\frac{e}{k_B T_e}\phi(\lambda_D x), \tag{8}$$

this one will be referred to as $X - y$ representation. To write down the model equations according to this representation in a dimensionless form, we multiply equations (1), (2) and (4) by the factors $\lambda_D(c_s n_{e0})^{-1}$, $\lambda_D(c_s^2 n_{e0} M_+)^{-1}$ and $\lambda_D^2(eK_B T_e)^{-1}$,

respectively, to obtain

$$\vec{\nabla}_X (N\vec{c}) = q_{\rm i} {\rm e}^{-y}, \tag{9a}$$

$$\left(\vec{c}\cdot\vec{\nabla}_X\right)\vec{c} - \vec{\nabla}_X y = q_{\rm b}\vec{c}\wedge\vec{b} - q_{\rm c}|\vec{c}|^{p+1}\vec{c} - q_{\rm i}\frac{{\rm e}^{-y}}{N}\vec{c}, \tag{9b}$$

$$\vec{\nabla}_X^2 y = N - {\rm e}^{-y}, \tag{9c}$$

where $\vec{b} = (\cos\theta, \sin\theta, 0)$ is the unitary vector co-linear to the magnetic field and $|\vec{c}| = (u^2 + v^2 + w^2)^{1/2}$. From these equations, the sheath solution, written as y_0, corresponds to $q_{\rm i} = q_{\rm c} = q_{\rm b} = 0$:

$$(Nu)\dot{} = 0, \tag{10a}$$

$$u\dot{u} - \dot{y} = 0, \tag{10b}$$

$$\ddot{y} = N - {\rm e}^{-y}, \tag{10c}$$

$$v = w = 0, \tag{10d}$$

where a dot means a derivative with respect to X. The sheath solution is universal in the sense that it does not depend on the pre-sheath mechanism to form the sheath.

3.2. Pre-sheath representation

For the real case $\lambda_{\rm D}/\lambda \neq 0$ many properties of the sheath are determined by the pre-sheath mechanism. To discuss these properties according to this mechanism, it is convenient to define the pre-sheath representation which will be characterized by the minimum length of the three: $\lambda_{\rm i}$, $\lambda_{\rm c}$ and $\lambda_{\rm b}$, i.e. $L = \lambda = \min\{\lambda_{\rm c}, \lambda_{\rm i}, \lambda_{\rm b}\}$ and the corresponding non-neutrality parameter $q = \lambda_{\rm D}/\lambda = \max\{q_{\rm c}, q_{\rm i}, q_{\rm b}\}$. This pre-sheath representation determines the electric field profile in the pre-sheath scale:

$$\xi = \frac{x}{\lambda}, \qquad \eta(\xi) = -\frac{e}{k_{\rm B}T_{\rm e}}\phi(\lambda\xi), \tag{11}$$

and will be referred to as $\xi - \eta$. In this case, to normalize equations (1), (2) and (4), we multiply both sides by the factors $\lambda(c_{\rm s}n_{\rm e0})^{-1}$, $\lambda(c_{\rm s}^2 n_{\rm e0}M_+)^{-1}$ and $\lambda^2(eK_{\rm B}T_{\rm e})^{-1}$ respectively:

$$\vec{\nabla}_\xi(N\vec{c}) = f_{\rm i}{\rm e}^{-\eta}, \tag{12a}$$

$$(\vec{c}\vec{\nabla}_\xi)\vec{c} - \vec{\nabla}_\xi\eta = f_{\rm b}\vec{c}\wedge\vec{b} - f_{\rm c}|\vec{c}|^{p+1}\vec{c} - f_{\rm i}\frac{{\rm e}^{-\eta}}{N}\vec{c}, \tag{12b}$$

$$q^2\vec{\nabla}_\xi^2\eta = N - {\rm e}^{-\eta}, \tag{12c}$$

where

$$f_{\rm i} = \frac{\lambda}{\lambda_{\rm i}} = \frac{q_{\rm i}}{q}, \qquad f_{\rm c} = \frac{\lambda}{\lambda_{\rm c}} = \frac{q_{\rm c}}{q}, \qquad f_{\rm b} = \frac{\lambda}{\lambda_{\rm b}} = \frac{q_{\rm b}}{q}. \tag{13}$$

If the non-neutrality parameter q gives us an idea of the deviation of the electric potential η from the quasi-neutral solution, the parameters $f_{\rm i}$, $f_{\rm c}$ and $f_{\rm b}$ give us information of the weight of each pre-sheath mechanism in this solution. In the following, to discuss the character of the pre-sheath, we define the two parameters:

$$\beta_{\rm i} = \frac{\lambda_{\rm b}}{\lambda_{\rm i}} = \frac{q_{\rm i}}{q_{\rm c}}, \qquad \beta_{\rm c} = \frac{\lambda_{\rm b}}{\lambda_{\rm c}} = \frac{q_{\rm c}}{q_{\rm b}}, \tag{14}$$

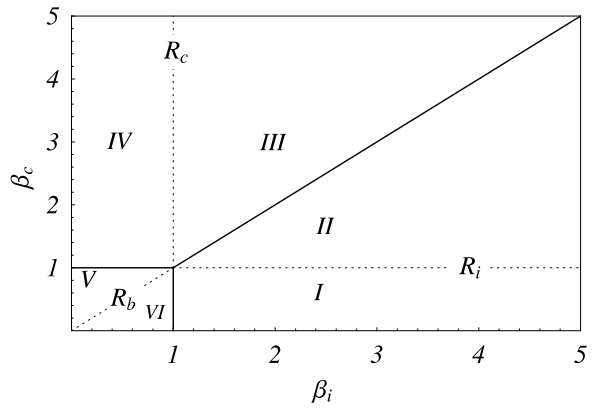

Figure 1. $\beta_{\rm i} \times \beta_{\rm c}$ plane. In region $R_{\rm i} \equiv I \cup II$ the dominant pre-sheath mechanism is ionization, in $R_{\rm c} \equiv III \cup IV$ are collisions, and finally in $R_{\rm b} \equiv V \cup VI$ magnetization.

if ionization increases over magnetization, then $\beta_{\rm i}$ increases, if collisions increase over magnetization, then $\beta_{\rm c}$ increases. Figure 1 represents a $\beta_{\rm i} \times \beta_{\rm c}$ plane which depicts six regions that correspond to the six possibilities to order the three lengths $\lambda_{\rm i}$, $\lambda_{\rm c}$ and $\lambda_{\rm b}$:

$$\begin{aligned}
I &\equiv [1,\infty)\times[0,1] & \lambda_{\rm i} < \lambda_{\rm b} < \lambda_{\rm c}\\
II &\equiv [1,\infty)\times[1,\beta_{\rm i}] & \lambda_{\rm i} < \lambda_{\rm c} < \lambda_{\rm b}\\
III &\equiv [1,\beta_{\rm c}]\times[1,\infty) & \lambda_{\rm c} < \lambda_{\rm i} < \lambda_{\rm b}\\
IV &\equiv [0,1]\times[1,\infty) & \lambda_{\rm c} < \lambda_{\rm b} < \lambda_{\rm i}\\
V &\equiv [1,\beta_{\rm c}]\times[0,1] & \lambda_{\rm b} < \lambda_{\rm c} < \lambda_{\rm i}\\
VI &\equiv [0,1]\times[0,\infty) & \lambda_{\rm b} < \lambda_{\rm i} < \lambda_{\rm c}.
\end{aligned}$$

From all of these regions, the three regions, which determine the prevailing pre-sheath mechanism to form the sheath, are

$$R_{\rm i} = I \cup II \tag{15a}$$

$$R_{\rm c} = III \cup IV. \tag{15b}$$

$$R_{\rm b} = V \cup VI \tag{15c}$$

in region $R_{\rm i}$, $\lambda = \lambda_{\rm i}$ and the pre-sheath is determined by ionization, in $R_{\rm c}$, $\lambda = \lambda_{\rm c}$ and the pre-sheath is mainly collisional, and finally in $R_{\rm b}$, the pre-sheath has a magnetic character and $\lambda = \lambda_{\rm b}$. We can express $f_{\rm i}$, $f_{\rm c}$, and $f_{\rm b}$ as functions of the parameters $\beta_{\rm i}$ and $\beta_{\rm c}$ into each region:

$$f_{\rm i}(\beta_{\rm i},\beta_{\rm c}) = \begin{cases} 1, & R_{\rm i}\\ \beta_{\rm i}/\beta_{\rm c}, & R_{\rm c}\\ \beta_{\rm i}, & R_{\rm b}\end{cases} \tag{16a}$$

$$f_{\rm c}(\beta_{\rm i},\beta_{\rm c}) = \begin{cases} \beta_{\rm c}/\beta_{\rm i}, & R_{\rm i}\\ 1, & R_{\rm c}\\ \beta_{\rm c}, & R_{\rm b}\end{cases} \tag{16b}$$

$$f_{\rm b}(\beta_{\rm i},\beta_{\rm c}) = \begin{cases} 1/\beta_{\rm i}, & R_{\rm i}\\ 1/\beta_{\rm c}, & R_{\rm c}\\ 1, & R_{\rm b}.\end{cases} \tag{16c}$$

Although, according to (12*a*)–(12*c*) η, N, and $\vec{c}$ depend on ξ, q, $\beta_{\rm i}$ and $\beta_{\rm c}$ we will only express their dependence on ξ,

i.e. $\vec{c} = \vec{c}(\xi) = (u(\xi), v(\xi), w(\xi))$, $\eta = \eta(\xi)$ and $N = N(\xi)$ and therefore, the scalar version of (12*a*)–(12*c*) is

$$(Nu)' = f_{\rm i} {\rm e}^{-\eta}, \tag{17a}$$

$$uu' - \eta' = -f_{\rm b} b_y w - f_{\rm c} |\vec{c}|^{p+1} u - f_{\rm i} \frac{{\rm e}^{-\eta}}{N} u, \tag{17b}$$

$$uv' = f_{\rm b} b_x w - f_{\rm c} |\vec{c}|^{p+1} v - f_{\rm i} \frac{{\rm e}^{-\eta}}{N} v \tag{17c}$$

$$uw' = f_{\rm b}(b_y u - b_x v) - f_{\rm c} |\vec{c}|^{p+1} w - f_{\rm i} \frac{{\rm e}^{-\eta}}{N} w \tag{17d}$$

$$q^2 \eta'' = N - e^{-\eta}, \tag{17e}$$

where $|\vec{c}| = (u^2 + v^2 + w^2)^{1/2}$, prime indicates derivation with respect to ξ, $b_x = \cos\theta$, and $b_y = \sin\theta$.

3.3. Solution of the model

The plasma or pre-sheath solution corresponds to the solution of (17*a*)–(17*e*) for which the quasi-neutrality condition holds, i.e. $N = {\rm e}^{-\eta}$. To obtain this pre-sheath solution, that will be named $\eta_0 = \eta_0(\xi)$, we make $q = 0$ in (17*a*)–(17*e*). From η_0, we can obtain the electric potential from the plasma to the wall $\eta(\xi)$, in the more realistic case when $q \neq 0$, assuming the quasi-neutrality condition in the plasma, i.e. $\eta \simeq \eta_0$ and $\eta' \simeq \eta_0'$ at $\xi \to 0$, where $u \to 0$.

3.3.1. Pre-sheath solution. For the pre-sheath solution, we can solve η_0' from (17*b*) by substitution of (17*a*) and the quasi-neutrality condition $N = {\rm e}^{-\eta_0}$:

$$\eta_0' = \frac{(2f_{\rm i} + f_{\rm c}|\vec{c}|^{p+1})u + f_{\rm b} b_y w}{1 - u^2}, \tag{18}$$

which becomes infinite at the point where $u = 1$. To avoid this infinity when $\eta_0(\xi)$ is calculated, we take as the independent variable, the x-component of the velocity of the positive ions u. Doing that in equations (17*a*)–(17*e*) together with $q = 0$ and $N = {\rm e}^{-\eta_0}$, we obtain the equations which determine the pre-sheath solution:

$$\dot{\xi} = \frac{1 - u^2}{f_{\rm i}(1+u^2) + f_{\rm c}|\vec{c}|^{p+1}u^2 + f_{\rm b} b_y w u}, \tag{19a}$$

$$\dot{v} = \left(\frac{u^2 - 1}{u}\right)\left[\frac{(f_{\rm i} + f_{\rm c}|\vec{c}|^{p+1})v - f_{\rm b} b_x w}{f_{\rm i}(1+u^2) + f_{\rm c}|\vec{c}|^{p+1}u^2 + f_{\rm b} b_y w u}\right], \tag{19b}$$

$$\dot{w} = \left(\frac{u^2 - 1}{u}\right)\left[\frac{(f_{\rm i} + f_{\rm c}|\vec{c}|^{p+1})w - f_{\rm b}(b_y u - b_x v)}{f_{\rm i}(1+u^2) + f_{\rm c}|\vec{c}|^{p+1}u^2 + f_{\rm b} b_y w u}\right], \tag{19c}$$

$$\dot{\eta_0} = \frac{(2f_{\rm i} + f_{\rm c}|\vec{c}|^{p+1})u + f_{\rm b} b_y w}{f_{\rm i}(1+u^2) + f_{\rm c}|\vec{c}|^{p+1}u^2 + f_{\rm b} b_y w u}, \tag{19d}$$

where $\dot{*} = {\rm d}*/{\rm d}u$. The initial conditions to solve (19*a*)–(19*d*) can be obtained assuming that in the plasma, where $\xi \to 0$, $\eta_0 \to 0$, $\eta_0' \to 0$, $\vec{c} \to 0$, the following series expansions are valid:

$$u = u_1 \xi + \cdots, \tag{20a}$$

$$v = v_1 \xi + \cdots, \tag{20b}$$

$$w = w_1 \xi + \cdots, \tag{20c}$$

$$\eta_0 = \eta_{02} \xi^2 + \cdots, \tag{20d}$$

or equivalently

$$\xi = u/u_1 + \cdots, \tag{21a}$$

$$v = (v_1/u_1)u + \cdots, \tag{21b}$$

$$w = (w_1/u_1)u + \cdots, \tag{21c}$$

$$\eta_0 = (\eta_{02}/u_1^2)u^2 + \cdots, \tag{21d}$$

where u_1, v_1, w_1 and η_{02} are constants to be determined. By substitution of these expressions (21*a*)–(21*d*) on (19*a*)–(19*d*) and taking into account only the first terms different from zero, we obtain

$$u_1 = f_{\rm i}, \tag{22a}$$

$$v_1 = \frac{f_{\rm i} f_{\rm b}^2 b_x b_y}{(2f_{\rm i} - pf_{\rm c})^2 + f_{\rm b}^2 b_x^2}, \tag{22b}$$

$$w_1 = \frac{f_{\rm i}(2f_{\rm i} - pf_{\rm c}) f_{\rm b} b_y}{(2f_{\rm i} - pf_{\rm c})^2 + f_{\rm b}^2 b_x^2}, \tag{22c}$$

$$\eta_{02} = \frac{f_{\rm i}(2f_{\rm i} - pf_{\rm c})}{2}\left(1 + \frac{f_{\rm b}^2 b_y^2}{(2f_{\rm i} - pf_{\rm c})^2 + f_{\rm b}^2 b_x^2}\right), \tag{22d}$$

where $p = 0$ for the constant collision mean free path case, and $p = -1$ for the constant collision frequency. If we take a sufficiently small (close to the plasma) initial value of $u = u_{\rm i}$, we can build up the initial conditions to solve (19*a*)–(19*d*) from (21*a*)–(21*d*) in the form $\xi_{\rm i} = \xi(u_{\rm i})$, $v_{\rm i} = v(u_{\rm i})$, $w_{\rm i} = w(u_{\rm i})$ and $\eta_{0i} = \eta_0(u_{\rm i})$.

3.3.2. Complete solution. If we consider a very small value of $u = u_{\rm i}$ (in our case $u_{\rm i} = 10^{-8}$) the above expressions can also be used to determine the complete solution of (17*a*)–(17*e*) for the case $q \neq 0$, because close to the plasma $\eta \simeq \eta_0 \to 0$ and $\eta' \simeq \eta_0' \to 0$. In this case, the initial conditions are obtained from

$$\xi = u/f_{\rm i}, \tag{23a}$$

$$v = \frac{f_{\rm i} f_{\rm b}^2 b_x b_y}{(2f_{\rm i}^2 - pf_{\rm c})^2 + f_{\rm b}^2 b_x^2}\xi, \tag{23b}$$

$$w = \frac{f_{\rm i}(2f_{\rm i}^2 - pf_{\rm c}) f_{\rm b} b_y}{(2f_{\rm i}^2 - pf_{\rm c})^2 + f_{\rm b}^2 b_x^2}\xi, \tag{23c}$$

$$\eta = \frac{f_{\rm i}(2f_{\rm i}^2 - pf_{\rm c})}{2}\left(1 + \frac{f_{\rm b}^2 b_y^2}{(2f_{\rm i}^2 - pf_{\rm c})^2 + f_{\rm b}^2 b_x^2}\right)\xi^2, \tag{23d}$$

$$\eta' = f_{\rm i}(2f_{\rm i}^2 - pf_{\rm c})\left(1 + \frac{f_{\rm b}^2 b_y^2}{(2f_{\rm i}^2 - pf_{\rm c})^2 + f_{\rm b}^2 b_x^2}\right)\xi \tag{23e}$$

$$N = {\rm e}^{-\eta}, \tag{23f}$$

and expressed as $u_{\rm i} = u(\xi_{\rm i})$, $v_{\rm i} = v(\xi_{\rm i})$, $w_{\rm i} = w(\xi_{\rm i})$, $\eta_{\rm i} = \eta(\xi_{\rm i})$, $\eta_{\rm i}' = \eta'(\xi_{\rm i})$ and $N_{\rm i} = N(\eta_{\rm i})$ figure 2 shows the plasma solution and the complete solution for a particular choice of the parameters p, $\beta_{\rm i}$, $\beta_{\rm c}$, θ, and different values of q. We can observe the boundary layer structure when $q \to 0$.

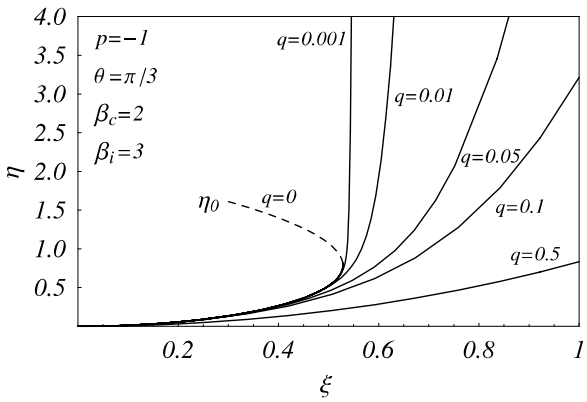

Figure 2. Pre-sheath and complete solutions of the model for several values of the non-neutrality parameter q.

4. Results of the model

In this section we analyse several properties of the sheath and the polarized wall such as the thickness of the sheath, the current to voltage characteristic curves, the saturation current collected by the wall and finally the floating potential. To obtain these results, (17*a*)–(17*e*) have been solved for different values of the parameters q, β_i and β_c.

4.1. Current to voltage characteristics

The current collected by the wall is determined by the x-component of the positive ion current density $j_x = Nu$. In this section, we analyse the effect of the different parameters on j_x. To this end, figures 3(*a*)–(*c*) represent j_x versus the electric potential of the wall η_p. As can be observed, with increasing β_c, j_x decreases and conversely, when β_i increases j_x increases. We can understand this behaviour if we consider the effect of each pre-sheath mechanism on j_x: (i) collisions cause a decrease in j_x due to the loss of momentum of the positive ions, (ii) ionization increases j_x because more positive ions are created in the pre-sheath and finally (iii) magnetization causes a decrease in j_x because more ions are deviated from the perpendicular direction to the wall. When β_i increases, ionization increases and/or magnetization decreases and consequently the net effect is that the positive ion current collected by the wall increases. When β_c increases, collisions increase and/or magnetization decreases. In this case, the effects of the two mechanisms are opposite. Figure 3, shows that j_x decreases as β_c increases, which indicates that collisions have a major effect than the magnetic field. Figures 3, also show that if β_i increases (increasing ionization) the characteristic curves for the different values of β_c are closest because ionization compensates the loss of momentum by collisions. Figures 4(*a*) and (*b*) represent the saturation current density collected $j_{x,\mathrm{sat}}$ when the electric potential of the wall is $\eta_p = 15$. As β_i increases, $j_{x,\mathrm{sat}}$ increases as well due to the increase in ionization and the decrease in the magnetic field. This increase in $j_{x,\mathrm{sat}}$ is reduced as β_c increases due to the collision effect. Finally, figures 5 represent $j_{x,\mathrm{sat}}$ for $\eta_p = 15$ versus θ and different combinations of β_i and β_c that correspond to the regions R_b ($\beta_i = 0.1$, $\beta_c = 0.1$), R_c ($\beta_i = 1$, $\beta_c = 10$) and R_i ($\beta_i = 10$, $\beta_c = 1$) represented in figure 1. When $(\beta_i, \beta_c) \in R_b$, the effect of θ is more evident and the saturation current density oscillates around the value corresponding to R_c ($\beta_i = 1$, $\beta_c = 10$).

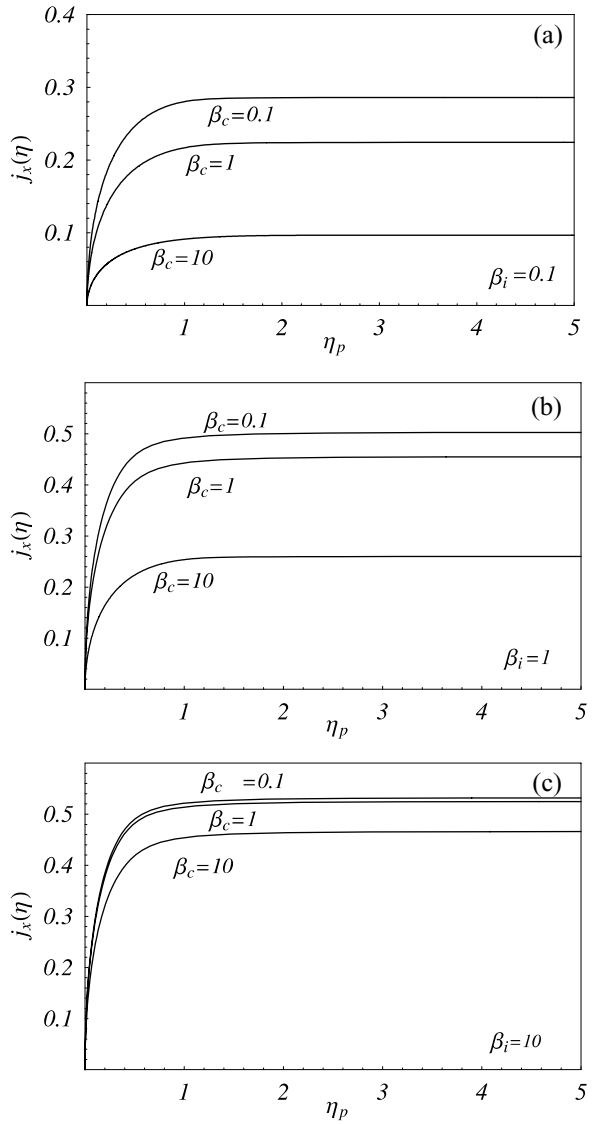

Figure 3. Positive current density versus the voltage of the wall for $p = -1$, $\theta = \pi/3$, $q = 0.01$ and different values of β_i and β_c.

4.2. Floating potential

The floating potential corresponds to the electric potential of the wall for which the net current density due to the positive ions and electrons is zero. Due to the smallness of the electron mass compared with the mass of the positive ions, this potential has to be a retarding potential for the electrons. It can be evaluated by solving the following equation:

$$j_x(\eta_f) = \sqrt{\frac{M}{2\pi m}} e^{-\eta_f} \tag{24}$$

where η_f is the floating potential of the wall. To obtain η_f for a particular choice of q, β_i and β_c, we first solve the model (17*a*)–(17*e*) and obtain $N(\xi)$, $u(\xi)$, and $\eta(\xi)$ and finally we

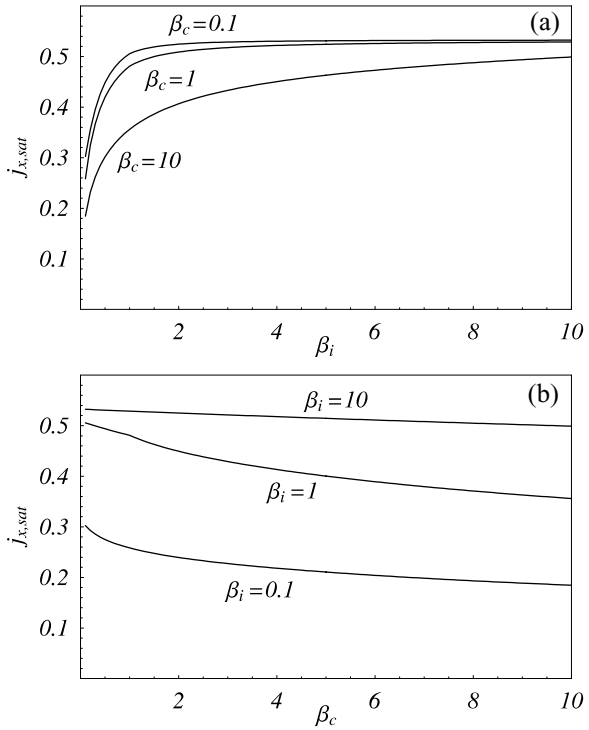

Figure 4. Saturation current density collected by the wall versus β_i and β_c for $p = 0, \theta = \pi/3, q = 0.01$ and $\eta_p = 15$.

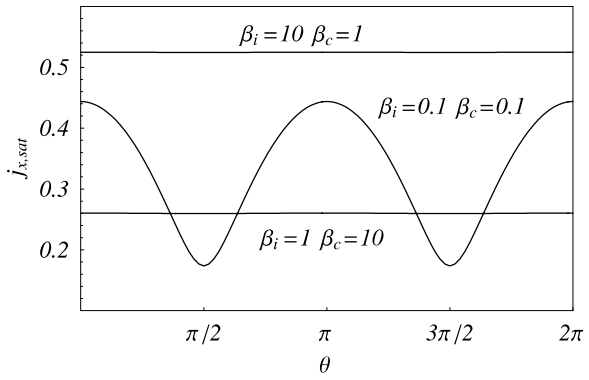

Figure 5. Saturation current density versus θ for $p = -1, q = 0.01$, $\eta_p = 15$ and three different values of β_i, β_c that correspond to a collisional pre-sheath (1, 10), a magnetic pre-sheath (0.1, 0.1) and an ionizing pre-sheath (10, 1).

solve equation (24) in the variable ξ:

$$N(\xi_f)u(\xi_f) = \sqrt{\frac{M}{2\pi m}}e^{-\eta(\xi_f)}, \tag{25}$$

finally the floating potential is obtained as $\eta_f = \eta(\xi_f)$. Figures 6(*a*) and (*b*) represent the dependence of η_f on β_i and β_c for the case of an argon plasma. As β_i increases, ionization increases and magnetization decreases. Both pre-sheath mechanisms tend to increase the positive current density and therefore, the electron-retarding potential or floating potential needed to reach a net current density equal to zero has to decrease. If β_c increases, collisions increase and magnetization decreases. Collisions increase j_x but magnetization decreases j_x. As can be observed in figure 6(*b*) the effect of collisions prevails over the magnetic-field effect.

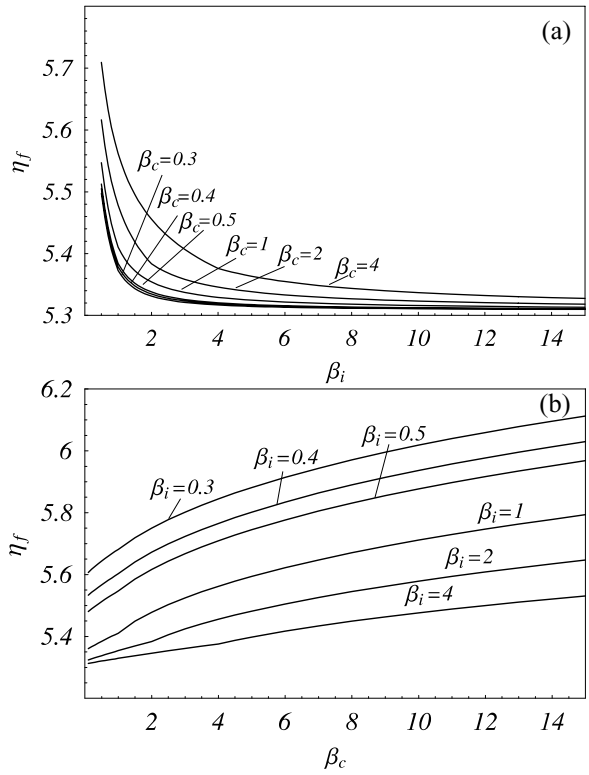

Figure 6. Floating potential versus β_i and β_c for $p = 0, \theta = \pi/3$ and $q = 0.01$.

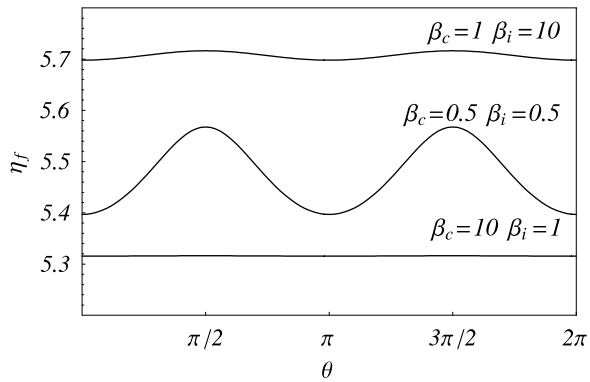

Figure 7. Floating potential versus θ for $p = 0, q = 0.01$ and three different values of (β_i, β_c).

This causes a decrease in j_x as was discussed in the previous section and therefore, the floating potential has to increase to get a zero current density collected by the wall. Figure 7 represents the dependence of η_f on θ. This dependence is appreciable when (β_i, β_c) $\in R_b$.

4.3. Sheath thickness

The sheath thickness is given by the distance between the point where the electric field of the plasma solution becomes infinite $\eta_0' \to \infty$ (this point will be called ξ_s) and the position of the conducting surface, that will be referred to as ξ_p,

$$\Delta\xi = \xi_p - \xi_s. \tag{26}$$

The point ξ_s can be found from the plasma solution by solving $\xi_s = \xi(u = 1)$ where $\xi(u)$ is obtained from

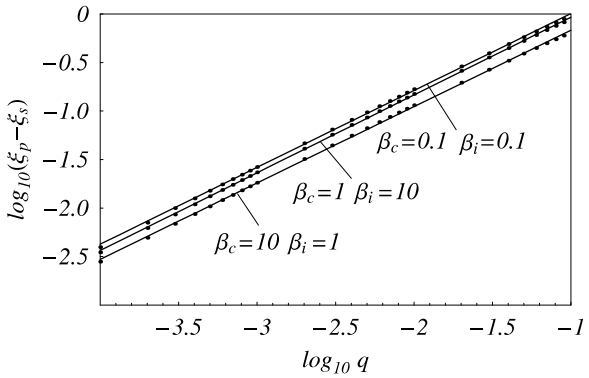

Figure 8. Sheath thickness versus q for $p = 0$, $\theta = \pi/3$ and $\eta_p = 5$ for a collisional pre-sheath $(\beta_i, \beta_c) = (1, 10)$, ionizing pre-sheath (10, 1) and a magnetic pre-sheath (0.1, 0.1). Dots represent the values obtained from the numerical solution of the model and lines correspond to the analytical fit according equation (27).

(19*a*)–(19*d*) and ξ_p by solving $\eta_p = \eta(\xi_p)$ once we have selected an arbitrary value of η_p, where $\eta(\xi)$ is obtained from the complete solution of equations (17*a*)–(17*e*).

The position and the electric potential of the wall are eigenvalues of the problem and therefore we can express $q = q(\xi_p, \eta_p, \beta_i, \beta_c)$. As has been shown in other papers [11–13] due to boundary layer structure of the sheath (see figure 2) the thickness of the sheath is of the order of $\lambda_D^{1-m}\lambda^m$ where λ is the characteristic length of the pre-sheath mechanism which determines the sheath formation and $0 < m < 1$. In dimensionless form

$$\Delta\xi = \delta_0 q^{1-m}, \tag{27}$$

where δ_0 is a constant. Figure 8 represents the sheath thickness in a log–log scale obtained from the numerical solution of the model. In the same figure, we have represented the analytical fit of the numerical result for different combinations of the parameters β_i and β_c which correspond to an ionizing pre-sheath $(\beta_i, \beta_c) = (10, 1)$, a collisional pre-sheath $(\beta_i, \beta_c) = (1, 10)$, and finally a magnetic pre-sheath $(\beta_i, \beta_c) = (0.1, 0.1)$. In all these cases the numerical results fit according to equation (27) and the corresponding coefficient $a_0 = \log_{10}\delta_0$, and $a_1 = \log_{10}(1 - m)$ are

(β_i, β_c)	a_0	a_1
0.1, 0.1	0.795 92	0.791 746
10, 1	0.770 205	0.802 189
1, 10	0.620 294	0.787 233

Figure 9 represents the dependence of the sheath thickness on the β_i and β_c parameters. To understand these figures we have to remember the effect of the three pre-sheath mechanisms on their capacity to shield the sheath: (i) ionization which increases the positive current density and helps one to shield the electric potential profile near the polarized wall, (ii) collisions which diminish the momentum of the positive ion fluid and prevents shielding of the potential profile and (iii) the magnetic field which deviates ions from the perpendicular direction to the polarized wall and also decreases the capacity to shield

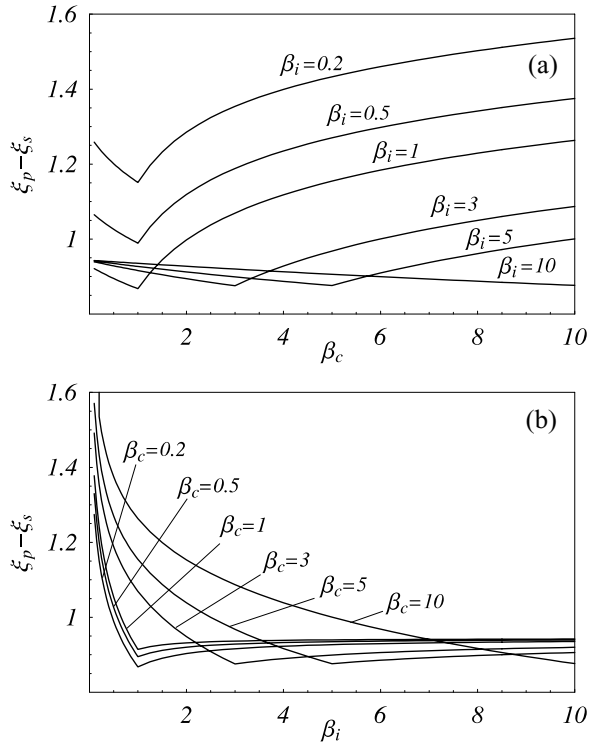

Figure 9. Sheath thickness versus β_i and β_c for $p = 0$, $\theta = \pi/3$, $q = 0.1$, and $\eta_p = 10$.

the electric potential. When β_i increases, ionization increases and/or magnetization decreases. When β_c increases, collisions increases and/or magnetization decreases. As can be observed in figure 9(*a*) when $\beta_i \leqslant 1$, there is always a qualitative change (a peak) in the sheath thickness which corresponds to a change in the prevailing pre-sheath mechanism (see figure 1 when β_c varies from R_b to R_c for a constant $\beta_i < 1$) from a magnetic pre-sheath to a collisional one. Before the peak, the sheath thickness decreases because as β_c increases, the magnetic field decreases and the capacity of the plasma to shield the electric potential profile increases. After the peak, the prevailing mechanism is collisions which diminish the capacity of the plasma to shield the sheath and consequently the sheath thickness increases. In the same figure, when $\beta_i > 1$, the peak in the sheath thickness happens for $\beta_c = \beta_i$ which corresponds to the transition from an ionizing pre-sheath to a collisional pre-sheath (see figure 1 when β_c varies from R_i to R_c for a constant $\beta_i > 1$). These results can be explained by considering that the three pre-sheath mechanisms are present in the model (17*a*)–(17*e*) through the coefficients f_c, f_i and f_b. If we draw a path in figure 1 from R_b to R_c with $\beta_i = \text{const} \leqslant 1$, then for $\beta_c < 1$, it is $f_c = \beta_c < 1$, $f_i = \beta_i < 1$, and $f_b = 1$ and the magnetic-field mechanism dominates. On the other hand, for $\beta_c > 1$, it is $f_c = 1$, $f_i = \beta_i/\beta_c < 1$ and $f_b = 1/\beta_c < 1$ and the prevailing mechanisms are collisions. The same reasoning can be followed for $\beta_i = \text{const} > 1$ when going from R_i to R_c and the magnetic mechanism is negligible. Figure 9(*b*) can be interpreted in the same way. Unlike what happens in figure 9(*a*), in the range $0 < \beta_i \leqslant 1$ and $\beta_c = \text{const} \leqslant 1$, the sheath thickness decreases more sharply because the two pre-sheath mechanisms involved as long as β_i increases are

the magnetic field and ionization which operate in the same direction, i.e. diminishing the sheath thickness as β_i increases.

5. Conclusions

In this paper, we have described what are the effects of ionization, ion–neutral collisions and magnetization on several properties of a negatively polarized wall in an electropositive plasma when the Boltzmann relation for electrons can be used. These properties are the saturation current density of the positive ions, the floating potential and the sheath thickness. The model is self-consistent and can be solved without imposing any criterion in addition to the quasi-neutrality condition in the plasma body. In general, all the results we have obtained can be understood by the effects that these three pre-sheath mechanisms have on the positive ion current. According to this, ionization, which is a source of positive ion current flowing to the wall, causes an increase in the saturation current density of the positive ions, a decrease in the floating potential required to equate the positive ion and electron currents and an increase in the capacity of the plasma to shield the electric potential close to the wall which causes a decrease in the sheath thickness. Collisions cause a loss of momentum of the positive ion fluid and therefore a decrease in the saturation current density collected by the wall, an increase in the electron-retarding floating potential to compensate the loss of momentum of the positive ions, and an increase in the sheath thickness due to the loss of capacity to shield the electric field of the wall. Finally, as magnetization causes a deviation of the positive ions from the perpendicular direction to the wall, as the magnetic-field strength increases, the saturation current collected diminishes, the floating potential increases and the sheath thickness also increases. In the case of the sheath thickness, we have also observed that it is very sensitive to the transition from a magnetic pre-sheath to an ionizing or collisional pre-sheath. When this transition happens, the qualitative behaviour of the sheath thickness also changes. We have also analysed all of these properties according to the orientation of the magnetic field, and the effect of this variable can only be appreciated in the case of a pre-sheath with a strong magnetic-field component. Finally, we have studied the sheath thickness according to the non-neutrality parameter λ_D/λ or the pre-sheath and sheath scales and we have shown, by fitting the numerical results, that it varies according to $\Delta z \propto \lambda^m \lambda_D^{1-m}$ where $m < 1$.

References

[1] Chodura R 1982 Plasma–wall transition in an oblique magnetic-field *Phys. Fluids* **25** 1628–33

[2] Riewmann K U 1994 Theory of the collisional presheath in an oblique magnetic-field *Phys. Plasmas* **1** 552–8

[3] Stangeby P C 1995 The Bohm–Chodura plasma sheath criterion *Phys. Plasmas* **2** 702–6

[4] Hutchinson I H 1996 The magnetic presheath boundary condition with $E \times B$ drifts *Phys. Plasmas* **3** 6–7

[5] Ahedo E 1997 Structure of the plasma–wall interaction in an oblique magnetic field *Phys. Plasmas* **4** 4419–30

[6] Beilis II and Keidar M 1998 Sheath and presheath structure in the plasma–wall transition layer in an oblique magnetic field *Phys. Plasmas* **5** 1545–53

[7] Sternberg N and Poggie J 2004 Plasma–sheath transition in the magnetized plasma–wall problem for collisionless ions *IEEE Trans. Plasma Sci.* **32** 2217–26

[8] Franklin R N 2005 The active magnetized plasma–sheath over a wide range of collisionality *J. Phys. D: Appl. Phys.* **38** 3412–6

[9] Allen J E 2008 The plasma boundary in a magnetic field *Contrib. Plasma Phys.* **48** 400–5

[10] Zimmermann T M G, Coppins M and Allen J E 2010 Coaxial discharge with axial magnetic field: Demonstration that the Boltzmann relation for electrons generally does not hold in magnetized plasmas *Phys. Plasmas* **17** 022301

[11] Crespo R M, Palop J I F, Ballesteros J, Hernandez M A, Lucena-Polonio M V and Diaz-Cabrera J M 2010 Study of sheath thickness in weakly ionized plasmas and its dependence on the electric potential and position of the probe *Plasma Sources Sci. Technol.* **19** 025012

[12] Crespo R M, Ballesteros J, Palop J I F, Hernandez M A, Lucena-Polonio M V and Diaz-Cabrera J M 2011 Study of the electropositive to electronegative sheath transition in weakly ionized plasmas *Plasma Sources Sci. Technol.* **20** 7

[13] Morales Crespo R, Ballesteros J, Fernandez Palop J I, Hernandez M A, Diaz-Cabrera J M, Lucena-Polonio M V and Tejero-del Caz A 2012 Boundary layer structure of the sheath surrounding a cylindrical or spherical probe in electronegative plasmas *Plasma Sources Sci. Technol.* **21** 055026